Vol. 26 • No. 37 • October 8 • 2014

www.advmat.de

ADVANCED MATERIALS

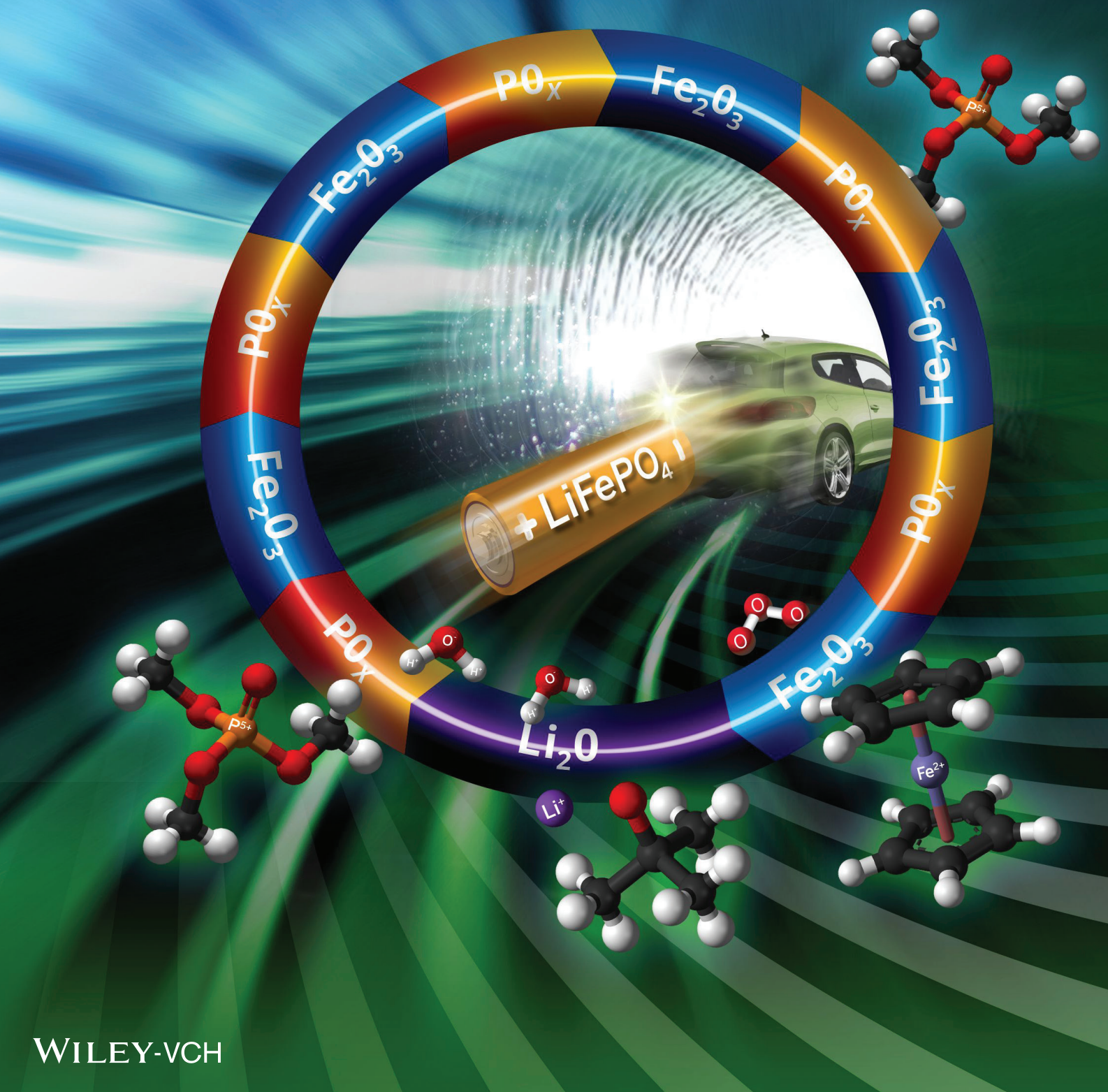

WILEY-VCH

ADVANCED MATERIALS
www.advmat.de

www.MaterialsViews.com

Rational Design of Atomic-Layer-Deposited $LiFePO_4$ as a High-Performance Cathode for Lithium-Ion Batteries

*Jian Liu, Mohammad N. Banis, Qian Sun, Andrew Lushington, Ruying Li, Tsun-Kong Sham, and Xueliang Sun**

Lithium transition metal phosphates ($LiMPO_4$, M = Fe, Mn, Co, Ni)[1] are enabling a new generation of high-power lithium-ion batteries (LIBs) that are instrumental in the worldwide effort to develop hybrid and plug-in hybrid electric vehicles. In particular, $LiFePO_4$ stands out as one of the most promising cathode materials, due to its high theoretical specific capacity (170 mA h g^{-1}), low cost, environmental friendliness, and intrinsic thermal stability.[2–4] However, pristine $LiFePO_4$ generally suffers from poor rate performance as a result of its sluggish mass- and charge-transport kinetics.[2–4] Tremendous effort over the past decade has shown that nanostructuring, along with coating/admixing with carbon and heteroatom doping, is an effective strategy toward overcoming the electronic- and ionic-conductivity limitations inherent to $LiFePO_4$, resulting in drastic improvements in its rate capability.[2–5] In these approaches, good control over the physical and chemical properties of nanostructured $LiFePO_4$ (such as morphology, size, composition, etc.,[6–8]) is critical in achieving optimal electrochemical performance. Accordingly, various methods have been developed to produce nanosized $LiFePO_4$, including solid-state reactions and solution chemistry (e.g., sol-gel, hydrothermal, spray pyrolysis, co-precipitation).[9–13]

Recently, atomic layer deposition (ALD) has emerged as an ideal technique toward engineering of nanostructures for a wide variety of applications, such as energy conversion and storage, microelectronics, sensing, etc.[14–16] ALD is a film-deposition technique based on the sequential use of self-terminating gas-solid surface reactions.[17,18] Due to the unique reaction-controlled deposition process utilized by ALD, it has the exceptional advantage of depositing uniform and conformal thin films on substrates with high-aspect-ratio topography, and provides high flexibility for tuning the size, thickness, and composition of target materials at the atomic scale.[14–16] Up to now, ALD has been widely adopted in LIBs to decorate the surface of active electrode materials with nanocoatings, thus improving their stability, capacity, and safety, etc. [19–22] Moreover, synthesis of electrode materials by ALD has been achieved for binary (such as SnO_2,[23] V_2O_5,[24] etc.) and ternary ($LiCoO_2$,[25] $LiMn_2O_4$,[26] $Li_4Ti_5O_{12}$[27,28]) systems, demonstrating tremendous potential use in conventional and 3D all-solid-state batteries.[21–23,26] However, to the best of our knowledge, there are still no reports on using the ALD technique to produce $LiMPO_4$ in the literature up to now. It has become more challenging to deposit quaternary materials rather than binary or ternary ones by ALD because of the more-complicated surface chemistry involved.[29]

Herein, for the first time, we develop an ALD approach to grow $LiFePO_4$, as a typical example of quaternary $LiMPO_4$ cathode materials, by carefully tailoring the surface reactions that occur. Distinguished from solid-state reactions and solution chemistries, the ALD approach employs self-limiting, vapor-based surface reactions to deposit $LiFePO_4$ in a layer-by-layer manner (Fe_2O_3, PO_x, and Li_2O subcycles). In this way, the ALD approach permits precise control over the thickness and film composition of $LiFePO_4$ at the atomic level. This unprecedented accuracy promises a versatile design of nanostructured $LiFePO_4$ on various types of substrates (in particular with high aspect ratio), and extends the employment of $LiFePO_4$ to a broader range of applications, especially in 3D all-solid state microbatteries for autonomous micro-devices. Moreover, $LiFePO_4$ is deposited on carbon nanotubes (CNTs) by ALD to form $LiFePO_4$/CNT nanocomposite, aiming at breaking through the rate-capability bottleneck typically for pristine $LiFePO_4$. Excitingly, the $LiFePO_4$/CNT electrode exhibits excellent rate capability, high power density, and ultra-long cycling lifetime, which are desirable properties for vehicular LIBs. Our work provides a new method for well-defined fabrication of high-powered cathode materials for rechargeable lithium batteries.

The ALD growth of $LiFePO_4$ is firstly verified on a Si (100) substrate. **Scheme 1** illustrates the ALD process employed in the deposition of amorphous $LiFePO_4$ at 300 °C with the use of ferrocene ($FeCp_2$), ozone (O_3), trimethylphosphate (TMPO), water (H_2O), and lithium *t*-butoxide (LiO^tBu) as precursors. The pulse times for $FeCp_2$, O_3, or TMPO are optimized in Fe_2O_3 or (Fe_2O_3 + PO_x) system to achieve saturated growth (Figure S1, Supporting Information). One ALD cycle of $LiFePO_4$ consists of 5 subcycles of (Fe_2O_3 + PO_x) and 1 subcycle of Li_2O, and is executed by the following sequence of 5 × [$FeCp_2$ (1 s pulse/10 s purge) + O_3 (1 s pulse/10 s purge) + TMPO (2 s pulse/10 s purge) + H_2O (1 s pulse/10 s purge)] + 1 × [LiO^tBu (1 s pulse/10 s purge) + H_2O (1 s pulse/10 s purge)]. Amorphous $LiFePO_4$ is obtained by repeating the above ALD cycle. The film thickness of amorphous $LiFePO_4$ on Si (100) substrate is linearly

J. Liu, M. N. Banis, Q. Sun, A. Lushington, R. Li, Prof. X. Sun
Department of Mechanical and Materials Engineering
University of Western Ontario
London, ON, N6A 5B9, Canada
E-mail: xsun@eng.uwo.ca
Prof. T.-K. Sham
Department of Chemistry
University of Western Ontario
ON, N6A 5B7, Canada

DOI: 10.1002/adma.201401805

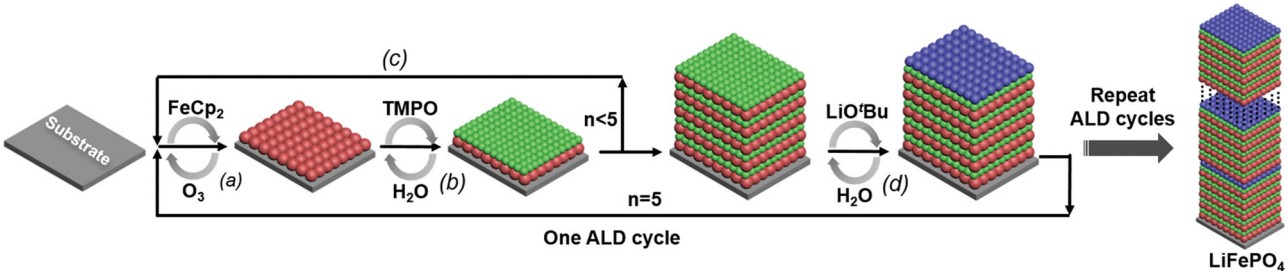

Scheme 1. Atomic layer deposition of amorphous $LiFePO_4$ at 300 °C using ferrocene ($FeCp_2$) ozone (O_3), trimethylphosphate (TMPO), water (H_2O), and lithium *t*-butoxide (LiO^tBu). a) Sequential pulse of $FeCp_2$ and O_3 leading to the growth of a Fe_2O_3 layer (red); b) sequential pulse of TMPO and H_2O leading to deposition of a PO_x layer (green); c) steps (a) and (b) are repeated for 5 times; d) sequential pulse of LiO^tBu and H_2O leading to formation of Li_2O layer (blue). One ALD cycle for the growth of amorphous $LiFePO_4$ consists of steps (a)–(d).

dependent with ALD cycle number, yielding a growth rate of ca. 0.94 nm/cycle (**Figure 1**). This linear relation between the film thickness and ALD cycle number indicates the self-limiting growth of $LiFePO_4$, a typical ALD-type deposition behavior.[17,18]

$LiFePO_4$ is then grown on CNTs using 140 ALD cycles to get $LiFePO_4$/CNT nanocomposite for structural and electrochemical characterizations. **Figure 2** demonstrates the morphology of the as-deposited and the annealed $LiFePO_4$/CNTs. Compared with the surface of pristine CNTs (Figure S2, Supporting Information), the exterior surface of CNTs is uniformly covered with $LiFePO_4$ after the ALD process (Figure 2a). Scanning transmission electron microscopy (STEM) imaging (Figure 2c) confirms the uniformity of the as-deposited $LiFePO_4$ layer with thickness of about 33 nm on the CNTs. After annealing in Ar gas for 5 h, the $LiFePO_4$ layer still coats the majority of the CNT surface. However, small portions of the underlying CNT surface are exposed, indicated by arrows in Figure 2b. The film thickness of the annealed $LiFePO_4$ layer on CNTs is measured to be around 20 nm in STEM image in Figure 2d. The reduced film thickness could result from the increase in film density, and the loss of film components, such as Li_2O[30] and possible residual ligands from ALD reactions,[27] during the annealing process. As-deposited $LiFePO_4$ on CNTs shows an amorphous phase in nature, as revealed by the diffusive rings in the selected area electron diffraction (SAED) pattern (inset in Figure 2c) and by the disordered structure observed in high resolution transmission electron microscopy (HRTEM) image (Figure S3, Supporting Information). On the contrary, annealed $LiFePO_4$ on CNTs displays distinct diffraction rings in its SAED pattern (inset in Figure 2d), suggesting a polycrystalline structure for the annealed $LiFePO_4$. Furthermore, HRTEM image of the annealed $LiFePO_4$ (Figure 2e) exhibits clear crystal planes with a d-spacing of 0.39 nm, corresponding to the (210) planes of orthorhombic $LiFePO_4$. Fe/P atomic ratio for the annealed $LiFePO_4$ is measured to be ca. 0.9 by energy dispersive spectroscopy (EDS) equipped with HRTEM (Figure S4, Supporting Information).

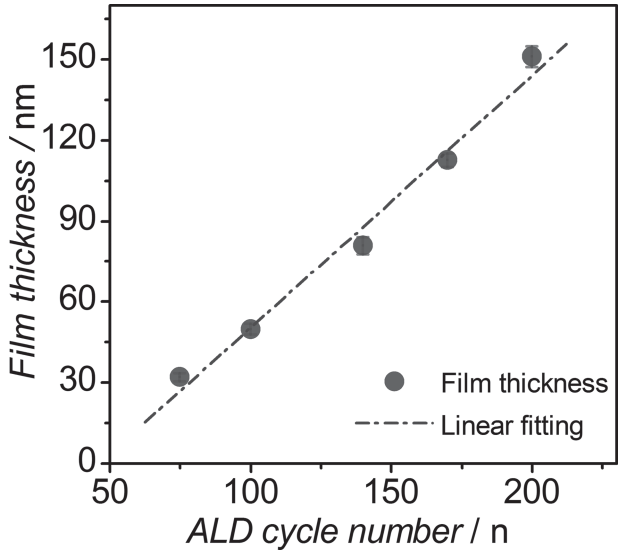

Figure 1. Linearity of amorphous $LiFePO_4$ film thickness vs. ALD cycle number, with a growth rate of (0.94 ± 0.08) nm/cycle.

Further analysis was conducted on the as-deposited and the annealed $LiFePO_4$/CNTs by X-ray diffraction (XRD) and X-ray absorption spectroscopy (XAS). As demonstrated in **Figure 3**a, the as-deposited $LiFePO_4$/CNTs displays only three XRD peaks, all of which can be attributed to CNTs (JCPDS No. 65–6212), with no indication of $LiFePO_4$, confirming that the as-deposited film is amorphous. In contrast, strong, sharp peaks, besides those from the CNTs, appear in the XRD pattern for the annealed $LiFePO_4$/CNTs, and can be well indexed as orthorhombic $LiFePO_4$ (JCPDS No. 83–2092) belonging to a *Pnma* space group. Interestingly, a few weak XRD peaks correlating to an Fe_3P impurity are detected in the annealed $LiFePO_4$/CNTs (Figure 3a). This iron phosphide impurity might be a result of carbothermal reduction of the $LiFePO_4$ phase by carbon or/and residual organic ligands in as-deposited $LiFePO_4$/CNTs during annealing, and had been proved to be beneficial to the battery performance of $LiFePO_4$ due to its high electronic conductivity.[31,32] The local electronic structure of $LiFePO_4$ is examined by X-ray absorption near-edge structure (XANES) analysis at the Fe K-edge, Fe $L_{2,3}$-edge, Li K-edge, and P $L_{2,3}$-edge. The Fe K-edge XANES spectrum of the annealed $LiFePO_4$ shows main edge and pre-edge peaks located at 7128 eV and around 7112 eV respectively, which correlate well with the peaks for standard crystalline $LiFePO_4$ (Figure 3b). The Fe pre-edge peak around 7112 eV represents the 1s → 3d transition,[33,34] indicating that Fe^{2+} predominates in the annealed $LiFePO_4$. For the as-deposited $LiFePO_4$, sharp Fe pre-edge peak located at about 7114 eV is evidence of Fe^{3+} in tetrahedral coordination.[33,34] The apparent shift toward lower energies in the main edge for the annealed $LiFePO_4$ is a result of a change in iron oxidation state from Fe^{3+} in as-deposited $LiFePO_4$ to Fe^{2+} in annealed $LiFePO_4$ (confirmed by Fe $L_{2,3}$-edge XANES result in Figure S5, Supporting Information). The Li K-edge XANES spectrum

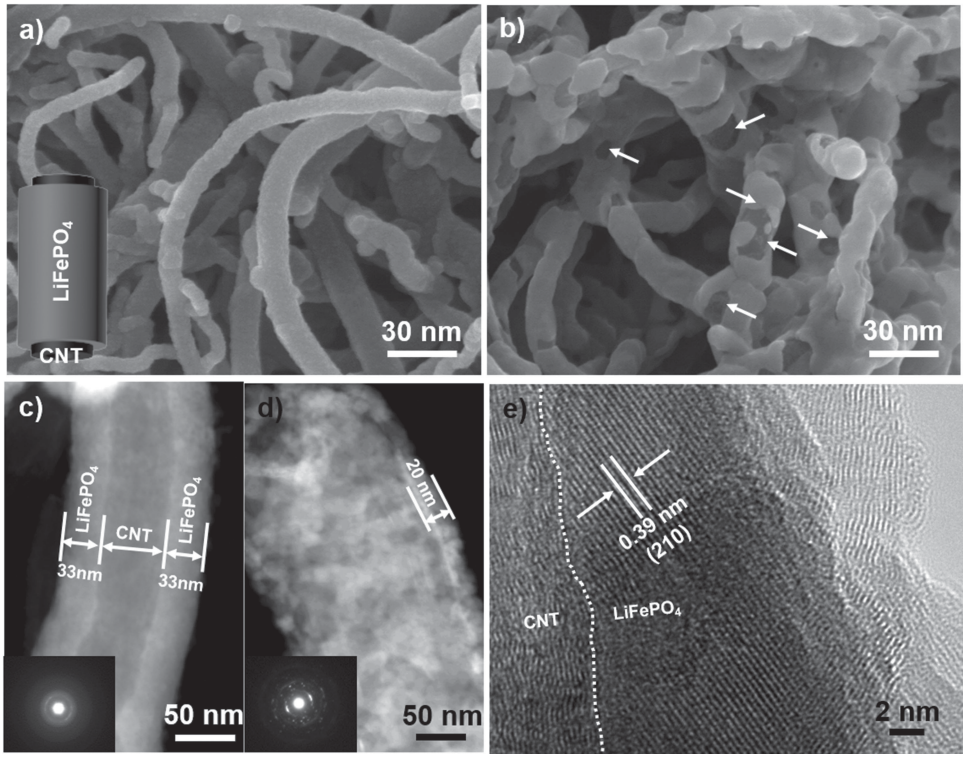

Figure 2. SEM images of: a) as-deposited $LiFePO_4$/CNTs and b) annealed $LiFePO_4$/CNTs; scanning transmission electron microscopy (STEM) images of: c) as-deposited $LiFePO_4$/CNTs and d) annealed $LiFePO_4$/CNTs (the insets in (c) and (d) are their corresponding selected area electron diffraction (SAED) patterns); e) high-resolution transmission electron microscopy (HRTEM) image of the annealed $LiFePO_4$/CNTs.

of the annealed $LiFePO_4$ exhibits all seven feature peaks as observed in reference crystalline $LiFePO_4$, albeit relatively weak intensities in peak C and D for the annealed $LiFePO_4$. It should be noted that the three peaks A′ (57.3 eV), B′ (54.9 eV), and C′ (52.1 eV) at lower energy are from Fe $M_{3,2}$-edges (3p-3d, 4s transitions).[35] Turning to the P $L_{2,3}$-edge, a typical doublet resonance (labelled as A and B in Figure 3d) is identified in the annealed $LiFePO_4$ and reference crystalline $LiFePO_4$. These two peaks are assigned to transitions from a spin-orbit split 2p electron into the first unoccupied 2s-like antibonding state.[35] In addition, a broad peak (peak C in Figure 3d) appears at ca. 2 eV higher photon energy in both samples. For the as-deposited $LiFePO_4$, a broadened white-line and extended features can be found in all the examined spectra (see Figure 3b,c,d and Figure S5, Supporting Information), indicating the as-deposited film is highly disordered, an observation consistent with HRTEM and XRD results. Similar spectroscopic features are observed in reference amorphous $LiFePO_4$ (see Figure S6, Supporting Information).

Figure 4 shows the electrochemical performance for the annealed $LiFePO_4$/CNT electrode for LIBs. As displayed in Figure 4a, a couple of redox peaks are observed at ca. 3.5 V and 3.3 V (vs Li/Li^+) in the cyclic voltammetry (CV) curve measured using a scan rate of 0.5 mV s^{-1}. These peaks correspond to the extraction and insertion of Li^+ in $LiFePO_4$.[36,37] These peaks are still clearly present in the voltage range of 2.5–4.2 V with increasing scan rate up to 20 mV s^{-1}, indicating the excellent electronic conductivity in the $LiFePO_4$/CNT electrode (as also revealed by the low charge-transfer resistance in the impedance spectrum in Figure S7 in the Supporting Information). The CNT network in the electrode is believed to be responsible for the good conductance.[38,39] The $LiFePO_4$/CNT electrode exhibits a discharge capacity of 150 mA h g^{-1} at 0.1 C (1 C = 170 mA g^{-1}) after several cycles, and can maintain high capacities at elevated current densities (Figure 4b). For example, it can still deliver a discharge capacity of 71 mA h g^{-1} at 60 C (10 200 mA g^{-1}, i.e. 1 min for each fully charging or discharging of the theoretical capacity), indicating its potential for high power output (Figure 4b). More importantly, the discharge capacity of the $LiFePO_4$/CNTs can be retrieved after cycling from 0.1 to 60 C (Figure 4c). The $LiFePO_4$/CNTs maintains almost the same rate performance when cycled from 0.1 to 60 C again (Figure S8, Supporting Information), demonstrating its excellent rate capability. The rate performance of $LiFePO_4$/CNTs prepared by ALD is comparable to that of high-rate $LiFePO_4$ composites prepared by other methods,[40–45] in particular at high rates of 30 C and 60 C (Figure S9, Supporting Information). Furthermore, the $LiFePO_4$/CNTs shows a stabilized discharge capacity as high as ca. 167 mA h g^{-1} (close to the theoretical capacity 170 mA h g^{-1} of $LiFePO_4$) after 100 cycles under a current density of 0.1 C (see inset in Figure 4d and Figure S8, Supporting Information). Moreover, the $LiFePO_4$/CNTs can maintain a discharge capacity of ca. 120 mA h g^{-1} after 2000 cycles at 1 C (170 mA g^{-1}), showing its extraordinary cyclic life. Overall, the remarkable performance of ALD-fabricated $LiFePO_4$/CNT cathode material could be ascribed to the following reasons: i) the unique and uniform nanostructure of $LiFePO_4$/CNTs synthesized by ALD enabling rapid Li^+ insertion and extraction; ii) improved electronic transfer between $LiFePO_4$ and CNTs; iii) fast ionic diffusion in the well-crystallized $LiFePO_4$;

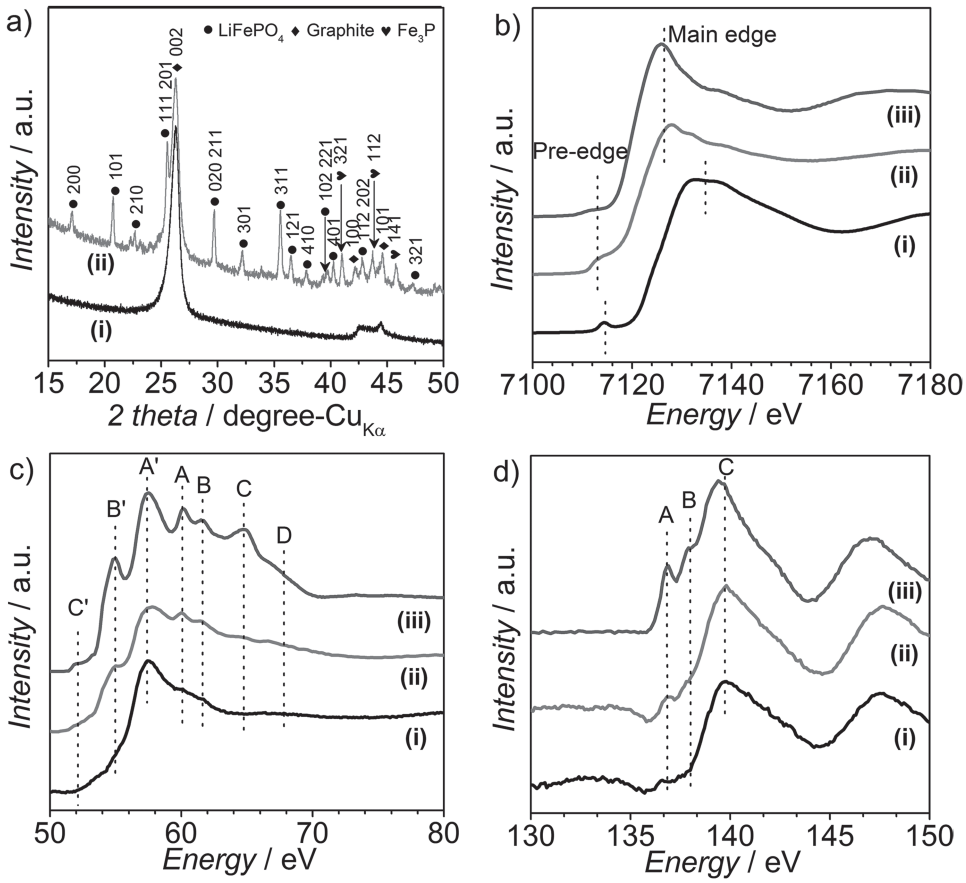

Figure 3. a) XRD patterns of as-deposited $LiFePO_4$/CNTs (i) and annealed $LiFePO_4$/CNTs (ii): (●) $LiFePO_4$, JCPDS No. 83–2092; (♦) Fe_3P, JCPDS No. 65–1606; (♥) graphite, JCPDS No. 65–6212; b) Fe K-edge, c) Li K-edge, and d) P $L_{3,2}$-edge X-ray absorption near-edge structure (XANES) spectra for as-deposited $LiFePO_4$/CNTs (i), annealed $LiFePO_4$/CNTs (ii), and reference crystalline $LiFePO_4$ (iii).

and iv) possibly enhanced electronic conductivity of the $LiFePO_4$/CNTs contributed from the conductive Fe_3P impurity.[31,32]

In summary, a $LiFePO_4$/CNT nanocomposite has been successfully synthesized using the ALD technique by a combination of Fe_2O_3, PO_x, and Li_2O subcycles. The annealed $LiFePO_4$/CNTs exhibited exceptional battery performance as a cathode material, including excellent rate capability, high power density, and long lifetime. These advantages make the $LiFePO_4$/CNT nanocomposite a competitive cathode material for the next generation of high-powered LIBs. Successful development of ALD process for $LiFePO_4$ promises it tremendous potential in 3D all-solid-state batteries.[25,26,46,47] Moreover, this ALD process allows coating of an ultrathin layer of $LiFePO_4$ on $LiMnPO_4$ to improve the carbon coating on the latter by taking advantage of the catalytic reaction of Fe with C, thus enhancing its battery performance.[48] In addition, this work establishes an suitable technique to customize $LiFePO_4$ model samples for fundamental studies,[16] owing to its excellent controllability over the crystallinity, thickness, composition, and morphology of $LiFePO_4$. The ALD strategy reported herein could also be extended to fabricate the other members of $LiMPO_4$ (M = Mn, Co, Ni), and thus paves a new way to synthesize complex cathode materials in a highly controllable fashion for rechargeable lithium batteries.

Experimental Section

Lithium iron phosphate ($LiFePO_4$) was grown at 300 °C in a Savannah 100 ALD system (Cambridge Nanotech.), by using ferrocene ($FeCp_2$) (98%, Sigma Aldrich), trimethylphosphate (TMPO) (97%, Strem Chemicals), lithium *t*-butoxide (LiO^tBu) (98%, Strem Chemicals), ozone (O_3) (ca. 9.8 wt%), and distilled water (H_2O) as precursors. All the chemicals were used as received. O_3 was generated in an OL80F generator from oxygen (O_2) (99.999%). The source temperatures for $FeCp_2$, TMPO, and LiO^tBu were 130 °C, 75 °C, and 180 °C, respectively. O_3 and H_2O were kept at room temperature (RT). One ALD cycle of $LiFePO_4$ was executed following the sequence of 5 × [$FeCp_2$ (1 s pulse/10 s purge) + O_3 (1 s pulse/10 s purge) + TMPO (2 s pulse/10 s purge) + H_2O (1 s pulse/10 s purge)] + 1 × [LiO^tBu (1 s pulse/10 s purge) + H_2O (1 s pulse/10 s purge)]. The pulse times for $FeCp_2$, O_3, and TMPO were optimized in Fe_2O_3 and (Fe_2O_3 + PO_x) systems, in order to achieve saturated growth of each layer (Figure S1, Supporting Information). The recipe for the Li_2O subcycle [LiO^tBu (1 s pulse/10 s purge) + H_2O (1 s pulse/10 s purge)] was taken from our previous work.[49] Carbon nanotubes (CNTs) (Shenzhen Nanotech.) and Si (100) wafer were used as the substrates for $LiFePO_4$. Before ALD growth, the CNTs were refluxed in nitric acid (HNO_3) (70%) for 3 h at 120 °C, in order to functionalize the surface of the CNTs and to remove residual Ni catalyst used for the growth of CNTs. The purified CNTs were well-dispersed in ethanol, and the mixture solution was dropped onto aluminum foil. Evaporation of ethanol resulted in a porous CNT network on the aluminum foil. In this way, the CNTs had maximum exposure to the precursors during the following ALD process, and therefore uniform

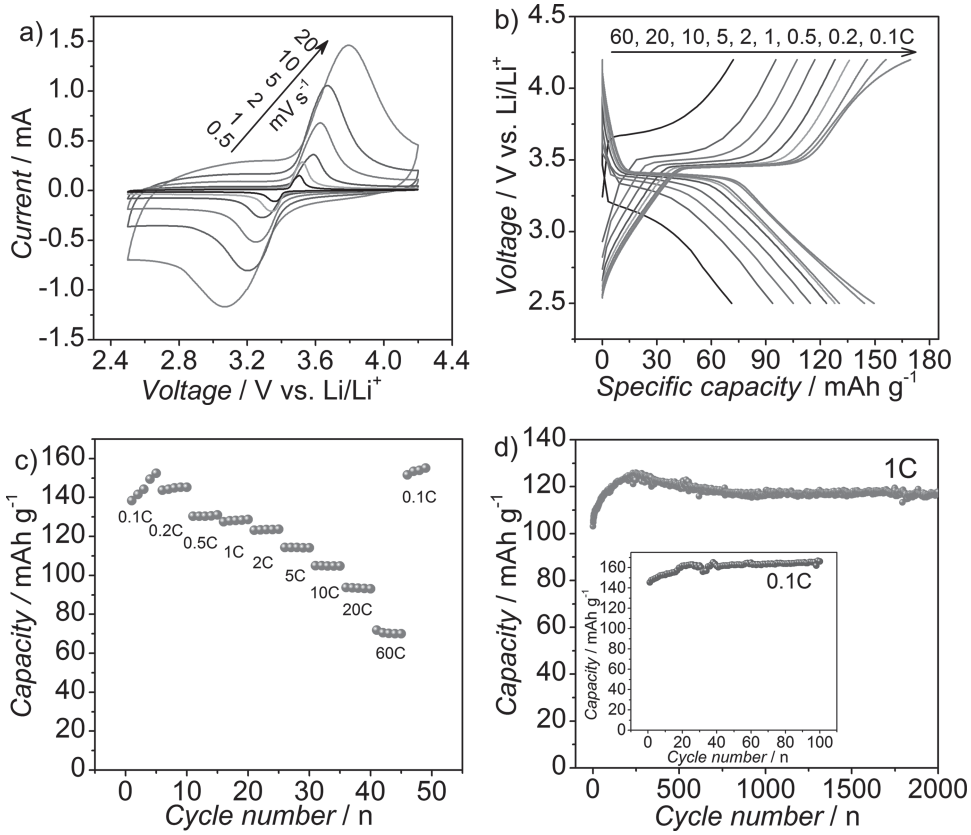

Figure 4. a) Cyclic voltammetry (CV) curves of annealed $LiFePO_4$/CNTs at scan rates of 0.5, 1, 2, 5, 10, and 20 mV s^{-1}; b) charge/discharge profiles and c) rate capability of the annealed $LiFePO_4$/CNTs at current densities of 0.1, 0.2, 0.5, 1, 2, 5, 10, 20, and 60 C; d) cycling stability of annealed $LiFePO_4$/CNTs measured at 1 C and 0.1 C.

coverage of $LiFePO_4$ on their surface. $LiFePO_4$/CNT nanocomposite was prepared by applying 140 ALD cycles of $LiFePO_4$ on the CNTs prepared as above. After ALD growth, the as-deposited $LiFePO_4$/CNTs were scratched from the aluminum foil, and subjected to annealing at 700 °C for 5 h under argon gas (99.999%) in order to obtain crystalline $LiFePO_4$. Annealed $LiFePO_4$/CNTs were used for electrochemical measurements. Si (100) wafer was cleaned with acetone three times, rinsed with ethanol, and subsequently blown dry with compressed air.

The morphology and structure of the as-deposited and annealed $LiFePO_4$/CNTs were characterized by using field-emission scanning electron microscopy (FESEM) (Hitachi S4800), high-resolution transmission electron microscopy (HRTEM) (JEOL 2010 FEG) equipped with energy dispersive spectroscopy (EDS), and an X-ray diffraction system (XRD) (Bruker D8 Advance, Cu Kα X-ray source), and X-ray absorption spectroscopy (XAS). XAS measurements were performed at the Canadian Light Source (CLS) on the Variable Line Spacing Plane Grating Monochromator (VLS PGM) beamline for Li-K edge and P $L_{2,3}$-edge spectra, the Spherical Grating Monochromator (SGM) beamline for the Fe $L_{2,3}$-edge spectra, and the Soft-X-ray Microcharacterization (SXRM) beamline for the Fe K-edge spectra. The loading of $LiFePO_4$ in the annealed $LiFePO_4$/CNT nanocomposite was measured by using thermogravimetric analysis (TGA) (SDT Q600) from RT to 800 °C in air at a heating rate of 10 °C min^{-1}. Si (100) substrates coated with $LiFePO_4$ using different ALD cycles were cut into small pieces to obtain fresh cross-section samples for thickness measurement under SEM.

Electrochemical performance of annealed $LiFePO_4$/CNTs was evaluated in coin-type half cells. To prepare the electrode, the annealed $LiFePO_4$/CNTs and poly(vinylidene fluoride) (PVDF) with a weight ratio of 90:10 were mixed thoroughly, and then the slurry was pasted onto an aluminum foil. The electrode was dried under vacuum at 100 °C overnight. The coin-type half cells were assembled in an argon-filled glove box ($[O_2]$ <1 ppm, $[H_2O]$ < 1 ppm), using the electrode prepared as above, polypropylene separator (Celgard 2400), and lithium foil as the counter electrode. The electrolyte was 1 M $LiPF_6$ solution in ethylene carbonate:diethyl carbonate:ethyl methyl carbonate (EC:DEC:EMC) with a volume ratio of 1:1:1. The electrochemical testing of the coin-type half cells was performed in an Arbin BT-2000 battery test system. The loading amount of $LiFePO_4$/CNTs on the electrode was ca. 1.5 mg. To show the efficiency of ALD-grown $LiFePO_4$, the specific capacity in this work was calculated based on the weight of only $LiFePO_4$, which was measured to be 18 wt% in the annealed $LiFePO_4$/CNTs by TGA (Figure S10, Supporting Information).

Supporting Information

Supporting Information is available from the Wiley Online Library or from the author.

Acknowledgements

This work was supported by Nature Sciences and Engineering Research Council of Canada (NSERC), Canada Research Chair (CRC) Program, Canada Foundation for Innovation (CFI), Ontario Research Fund (ORF), the Canada Light Source (CLS) at University of Saskatchewan, the Canadian Centre for Electron Microscopy (CCEM) at McMaster University, and University of Western Ontario. J.L. is grateful to the Mitacs Elevate Postdoctoral Fellowship program.

Received: April 21, 2014
Revised: May 23, 2014
Published online: July 8, 2014

[1] L. Dimesso, C. Förster, W. Jaegermann, J. P. Khanderi, H. Tempel, A. Popp, J. Engstler, J. J. Schneider, A. Sarapulova, D. Mikhailova, L. A. Schmitt, S. Oswald, H. Enrenberg, *Chem. Soc. Rev.* **2012**, *41*, 5068.
[2] L. X. Yuan, Z. H. Wang, W. X. Zhang, X. L. Hu, J. T. Chen, Y. H. Huang, J. B. Goodenough, *Energy Environ. Sci.* **2011**, *4*, 269.
[3] Y. Wang, P. He, H. Zhou, *Energy Environ. Sci.* **2011**, *4*, 805.
[4] J. Wang, X. Sun, *Energy Environ. Sci.* **2012**, *5*, 5163.
[5] H. Liu, Q. Cao, L. J. Fu, C. Li, Y. P. Wu, H. Q. Wu, *Electrochem. Commun.* **2006**, *8*, 1553.
[6] L. Wang, X. He, W. Sun, J. Wang, Y. Li, S. Fan, *Nano Lett.* **2012**, *12*, 5632.
[7] K. Saravanan, M. V. Reddy, P. Balaya, H. Gong, B. V. R. Chowdari, J. J. Vittal, *J. Mater. Chem.* **2009**, *19*, 605.
[8] N. Meethong, Y. H. Kao, S. A. Speakman, Y. M. Chiang, *Adv. Funct. Mater.* **2009**, *19*, 1060.
[9] A. K. Padhi, K. S. Nanjundaswamy, J. B. Goodenough, *J. Electrochem. Soc.* **1997**, *144*, 1188.
[10] R. Dominko, M. Bele, M. Gaberscek, M. Remskar, D. Hanzel, J. M. Goupil, S. Pejovnik, J. Jamnik, *J. Power Sources* **2006**, *153*, 274.
[11] S. Yang, P. Y. Zavalij, M. S. Whittingham, *Electrochem. Commun.* **2001**, *3*, 505.
[12] M. R. Yang, T. H. Teng, S. H. Wu, *J. Power Sources* **2006**, *159*, 307.
[13] G. Arnold, J. Garche, R. Hemmer, S. Ströbele, C. Vogler, M. Wohlfahrt-Mehrens, *J. Power Sources.* **2003**, *119–121*, 247.
[14] N. Pinna, M. Knez, in *Atomic Layer Deposition of Nanostructured Materials*, Wiley-VCH, Weinheim, Germany **2012**.
[15] C. Marichy, M. Bechelany, N. Pinna, *Adv. Mater.* **2012**, *24*, 1017.
[16] M. Knez, K. Nielsch, L. Niinistö, *Adv. Mater.* **2007**, *19*, 3425.
[17] R. L. Puurunen, *J. Appl. Phys.* **2005**, *97*, 121301.
[18] S. M. Geroge, *Chem. Rev.* **2010**, *110*, 111.
[19] I. D. Scott, Y. S. Jung, A. S. Cavanagh, Y. Yan, A. C. Dillon, S. M. George, S. H. Lee, *Nano Lett.* **2011**, *11*, 414.
[20] Y. S. Jung, A. S. Cavanagh, L. A. Riely, S. H. Kang, A. C. Dillon, M. D. Groner, S. M. George, S. H. Lee, *Adv. Mater.* **2010**, *22*, 2172.
[21] H. C. M. Knoops, M. E. Donders, M. C. M. van de Sanden, P. H. L. Notten, W. M. M. Kessels, *J. Vac. Sci. Technol. A* **2012**, *30*, 010801.
[22] X. Meng, X. Q. Yang, X. Sun, *Adv. Mater.* **2012**, *24*, 3589.
[23] X. Li, X. Meng, J. Liu, D. Geng, Y. Zhang, M. N. Banis, Y. Li, J. Yang, R. Li, X. Sun, M. Cai, M. W. Verbrugge, *Adv. Funct. Mater.* **2012**, *22*, 1647.
[24] X. Chen, E. Pomerantseva, P. Banerjee, K. Gregorczyk, R. Ghodssi, G. Rubloff, *Chem. Mater.* **2012**, *24*, 1255.
[25] M. E. Donders, W. M. Arnoldbik, H. C. M. Knoops, W. M. M. Kessels, P. H. L. Notten, *J. Electrochem. Soc.* **2013**, *160*, A3066.
[26] V. Miikkulainen, A. Ruud, E. Østreng, O. Nilsen, M. Laitinen, T. Sajavaara, H. Fiellvåg, *J. Phys. Chem. C* **2014**, *118*, 1258.
[27] V. Miikkulainen, O. Nilsen, M. Laitinen, T. Sajavaara, H. Fiellvåg, *RSC Adv.* **2013**, *3*, 7537.
[28] X. Meng, J. Liu, X. Li, M. N. Banis, J. Yang, R. Li, X. Sun, *RSC Adv.* **2013**, *3*, 7285.
[29] T. Aaltonen, M. Alnes, O. Nilsen, L. Costelle, H. Fjellvåg, *J. Mater. Chem.* **2010**, *20*, 2877.
[30] J. Wang, J. Yang, Y. Tang, J. Liu, Y. Zhang, G. Liang, M. Gauthier, Y. K. Chen-Wiegart, M. N. Banis, R. Li, J. Wang, T. K. Sham, X. Sun, *Nat. Commun.* **2014**, *5*, 3415.
[31] Y. H. Rho, L. F. Nazar, L. Perry, D. Ryan, *J. Electrochem. Soc.* **2007**, *154*, A283.
[32] P. S. Herle, B. Bellis, N. Cooms, L. F. Nazar, *Nature* **2004**, *3*, 147.
[33] A. A. M. Prince, S. Mylswamy, T. S. Chan, R. S. Liu, B. Hannoyer, M. Jean, C. H. Shen, S. M. Huang, J. F. Lee, G. X. Wang, *Solid State Commun.* **2004**, *132*, 455.
[34] A. Deb, U. Bergmann, S. P. Cramer, E. J. Cairns, *Electrochim. Acta.* **2005**, *50*, 5200.
[35] S. Yang, D. Wang, G. Liang, Y. M. Yiu, J. Wang, L Liu, X. Sun, T. K. Sham, *Energy Environ. Sci.* **2012**, *5*, 7007.
[36] X. L. Wu, L. Y. Jiang, F. F. Cao, Y. G. Guo, L. J. Wan, *Adv. Mater.* **2009**, *21*, 2710.
[37] W. J. Zhang, *J. Electrochem. Soc.* **2010**, *157*, A1040.
[38] W. Tang, X. Gao, Y. Zhu, Y. Yue, Y. Shi, Y. Wu, K. Zhu, *J. Mater. Chem.* **2012**, *22*, 20143.
[39] J. Yang, J. Wang, X. Li, D. Wang, J. Liu, G. Liang, M. Gauthier, Y. Li, D. Geng, R. Li, X. Sun, *J. Mater. Chem.* **2012**, *22*, 7537.
[40] Y. S. Hu, Y. G. Guo, R. Dominko, M. Gaberscek, J. Jamnik, J. Maier, *Adv. Mater.* **2007**, *19*, 1963.
[41] G. Wang, H. Liu, J. Liu, S. Qiao, G. M. Lu, P. Munroe, H. Ahn, *Adv. Mater.* **2010**, *22*, 4944.
[42] C. Sun, S. Rajasekhara, J. B. Goodenough, F. Zhou, *J. Am. Chem. Soc.* **2011**, *133*, 2132.
[43] S. W. Oh, S. T. Myung, S. M. Oh, K. H. Oh, K. Amine, B. Scrosati, Y. K. Sun, *Adv. Mater.* **2010**, *22*, 4842.
[44] S. W. Oh, S. T. Myung, H. J. Bang, C. S. Yoon, K. Amine, Y. K. Sun, *Electrochem. Solid-State Lett.* **2009**, *12*, A181.
[45] W. Tang, Y. Hou, F. Wang, L. Liu, Y. Wu, K. Zhu, *Nano Lett.* **2013**, *13*, 2036.
[46] J. F. M. Qudenhoven, L. Baggetto, P. H. L. Notten, *Adv. Energy Mater.* **2011**, *1*, 10.
[47] H. C. M. Knoops, M. E. Donders, L. Baggetto, M. C. M. van de Sanden, P. H. L. Notten, W. M. M. Kessels, *ECS Trans.* **2009**, *25*, 333.
[48] K. Zaghib, M. Trudeau, A. Guerfi, J. Trottier, A. Mauger, R. Veillette, C. M. Kulien, *J. Power Source.* **2012**, *204*, 177.
[49] J. Liu, M. N. Banis, X. Li, A. Lushington, M. Cai, R. Li, T.-K. Sham, X. Sun, *J. Phys. Chem. C.* **2013**, *117*, 20260.